Annals of Biomedical Engineering, Vol. 46, No. 7, July 2018 *(© 2018)* pp. 1001–1012
https://doi.org/10.1007/s10439-018-2022-x

Inter-subject FDG PET Brain Networks Exhibit Multi-scale Community Structure with Different Normalization Techniques

MEGAN M. SPERRY,[1] SONIA KARTHA,[1] ERIC J. GRANQUIST,[2] and BETH A. WINKELSTEIN[1,3,4]

[1]Department of Bioengineering, University of Pennsylvania, Philadelphia, PA 19104, USA; [2]Oral & Maxillofacial Surgery, University of Pennsylvania School of Medicine, Philadelphia, PA 19104, USA; [3]Department of Neurosurgery, University of Pennsylvania, Philadelphia, PA 19104, USA; and [4]240 Skirkanich Hall, 210 S. 33rd St., Philadelphia, PA 19104, USA

(Received 7 November 2017; accepted 30 March 2018; publication Online 11 April 2018)

Associate Editor Xiaoxiang Zheng oversaw the review of this article.

Abstract—Inter-subject networks are used to model correlations between brain regions and are particularly useful for metabolic imaging techniques, like 18F-2-deoxy-2-(18F)fluoro-D-glucose (FDG) positron emission tomography (PET). Since FDG PET typically produces a single image, correlations cannot be calculated over time. Little focus has been placed on the basic properties of inter-subject networks and if they are affected by group size and image normalization. FDG PET images were acquired from rats ($n = 18$), normalized by whole brain, visual cortex, or cerebellar FDG uptake, and used to construct correlation matrices. Group size effects on network stability were investigated by systematically adding rats and evaluating local network connectivity (node strength and clustering coefficient). Modularity and community structure were also evaluated in the differently normalized networks to assess meso-scale network relationships. Local network properties are stable regardless of normalization region for groups of at least 10. Whole brain-normalized networks are more modular than visual cortex- or cerebellum-normalized network ($p < 0.00001$); however, community structure is similar at network resolutions where modularity differs most between brain and randomized networks. Hierarchical analysis reveals consistent modules at different scales and clustering of spatially-proximate brain regions. Findings suggest inter-subject FDG PET networks are stable for reasonable group sizes and exhibit multi-scale modularity.

Keywords—Networks, Brain, FDG PET, Modularity.

INTRODUCTION

Network analysis has emerged as an important tool to measure both normal and pathological brain function, modeling the brain as an interconnected circuit instead of discrete regions with autonomous function.[34] Although some aspects of the brain's function are isolated to a single region or several brain regions, many critical functions involve sub-circuits or entire networks of brain regions. For example, brain network (BN) level changes are implicated in learning and memory,[8] sensation,[2] and chronic diseases like Alzheimer's disease.[14] Those studies have used many imaging techniques, including functional magnetic resonance imaging (fMRI) and 2-deoxy-2-(18F)fluoro-D-glucose (^{18}F-FDG) positron emission tomography (PET) to measure cellular function in the brain.[2,13,44] Imaging data are transformed into functional networks which serve as representative frameworks for topological relationships between brain regions.[2,13,44] BNs are constructed using either inter-regional correlation coefficients from brain activity recorded over time[2] or generated from brain activity across multiple subjects in the same experimental group.[13] Although functional networks derived from time-series data have well-defined properties and methods for network construction,[41] the methodological challenges associated with inter-subject network construction have not been defined.

FDG is a glucose analogue used to assess brain activity since it measures synaptic glutamatergic activity.[39] In mammals, a substantial portion of resting state glucose uptake supports synaptic activity, with neurons taking up more glucose than other cells in the central nervous system.[24,26] Unlike fMRI and other image measurements collected on the order of seconds, a single PET image typically represents cumulative brain activity over minutes-to-hours.[33] Since regions with highly correlated levels of brain activity are assumed to be functionally coupled,[13,30,44] inter-subject correlation matrices are constructed from regional

Address correspondence to Beth A. Winkelstein, 240 Skirkanich Hall, 210 S. 33rd St., Philadelphia, PA 19104, USA. Electronic mail: winkelst@seas.upenn.edu

measurements of metabolic activity to measure the relationship between brain regions. Network analyses of metabolic data have elucidated the effect of ketamine treatment on brain hubs,[13] established the role of astrocytic transporters in metabolic synchronicity across the brain,[44] and identified stronger connectivity and efficiency in right-sided compared to left-sided temporal lobe epilepsy.[42] Despite strong evidence of biologically-relevant network changes in those studies, the structure of inter-subject networks has not been investigated, nor have group size and variability been evaluated.

Community structure, which is the clustering of regions into groups that are highly associated with each other and less connected to all other nodes in the network, is a hallmark of BNs.[9] Since there is a trade-off between efficiency of information transfer and axonal wiring costs in the brain, modular network structure is hypothesized as allowing the efficient spread of information through brain circuitry.[9,29] Since modular architecture has been demonstrated in fMRI,[37] electrocorticography,[22] and anatomical BNs,[11,19] metabolic BNs are expected to exhibit similar organizational patterns. Even though modular architecture persists across different types of BNs, the composition and size of these modules is flexible; the brain's functional organization can be altered by differential inputs.[8] Disease[14] and aging[29] can disrupt brain community structure, suggesting that the normal integration and transfer of information is also altered in those states. Because both anatomical and functional BNs demonstrate flexible community structure, FDG PET networks are also hypothesized to have flexible modular architecture. However, this aspect of FDG PET network structure is currently unstudied.

This study investigated the resting state properties of FDG PET inter-subject networks in the rat to measure the metabolic relationships between brain regions. Node strength, clustering coefficient, and modularity were computed to evaluate the local and global properties of FDG PET BNs. Network diagnostics were measured for groups with different sizes to investigate the contribution of group size to network diagnostics and to determine if there is a critical group size for which networks stabilize. Although FDG PET images are also commonly intensity-normalized to correct for any variability in the dose of FDG, normalization techniques differ.[15,21,24] Network properties were measured for different types of image normalization to assess if, and how, network measurements change by normalization strategy. To this end, FDG uptake was normalized by whole brain activity, which is used to standardize PET images before further analysis.[15,23,24] In addition, PET images were separately normalized to the cerebellum, which is often used in studies of dementia because it is the brain region least affected by disease,[21] and the visual cortex, a region minimally impacted by disorders that are commonly studied using BN techniques.

MATERIALS AND METHODS

PET Imaging

All procedures were approved by the Institutional Animal Care and Use Committee at the University of Pennsylvania. Experiments were performed using female Holtzman rats (Envigo; Indianapolis, IN) weighing 275±25 g at the start of the study. Rats were housed with conditions recommended by the Association for Assessment and Accreditation of Laboratory Animal Care with a 12/12 h light/dark cycle, environmental enrichment, and free access to food and water.

Rats ($n = 18$) were injected with ^{18}F-FDG, manufactured by the University of Pennsylvania Cyclotron Facility, *via* tail vein catheter (800–1400 μCi at a volume < 2 mL) under brief exposure to isoflurane inhalation anesthesia (4% induction; 2% maintenance) and subsequently transitioned to dexmedetomidine sedation (0.075 mg/kg in 2 mL of 0.9% saline; DEXDOMITOR, Zoetis; Parsippany, NJ). Rats were kept under sedation for 1 h before PET imaging. Three-dimensional (3D) PET images were acquired in the resting state using a Philips MOSAIC HP Small Animal PET scanner (15-min single-frame acquisition) and were transferred to isolated housing until radioactivity was below detectable limits.

Image Processing

PET images were reconstructed into a 128 × 128 × 120 matrix with a voxel size of 1 mm × 1 mm × 1 mm. Image volumes were cropped around the head and spatially normalized to the Small Animal Molecular Imaging Toolbox (SAMIT) ^{18}F-FDG template[17] using linear, 6 degree-of-freedom image registration (Advanced Normalization Tools)[1] and re-sliced (0.2 mm × 0.2 mm × 0.2 mm). Brain volumes were segmented into 50 regions using the Schwarz stereotaxic rat brain atlas, with brain regions defined using anatomical T2-weighted MRI scans.[36,43] Collectively, the regions cover the entire brain which allows construction of a global BN. The Schwarz atlas contains composite and individual structures that are important to brain function, including cortical regions, limbic structures, and brainstem areas (Table 1). Mean ^{18}F-FDG PET uptake was calculated across all voxels within the combined left and right sides of each brain region of each rat. The mean ^{18}F-FDG uptake in each

TABLE 1. SAMIT brain regions and volumes.[17]

Brain region	Volume (mm^3)
Nucleus accumbens—core	7.4
Nucleus accumbens—shell	7.5
Amygdala	40.8
Nucleus stria terminalis	4.6
Caudate/putamen	86.7
Corpus collosum	61.3
Cortex—auditory	27.2
Cortex—cingulate	17.6
Cortex—entorhinal	48.9
Cortex—frontal association	9.8
Cortex—insular	34.2
Cortex—medial prefrontal	13.9
Cortex—motor	86.8
Cortex—orbitofrontal	24.5
Cortex—parietal association	11.9
Cortex—piriform	46.5
Cortex—retrosplenial	34.3
Cortex—somatosensory	158.8
Cortex—temporal association	12.0
Cortex—visual	69.5
Diagonal band	3.9
Globus pallidus	7.7
Hippocampus—anterodorsal	19.0
Hippocampus—posterior	4.3
Hippocampus—posterodorsal	35.2
Hippocampus—subiculum	23.1
Hippocampus—ventral	27.9
Hypothalamus—lateral	11.2
Hypothalamus—medial	25.6
Internal capsule	16.1
IPAC	2.7
Medial geniculate	3.2
Mesencephalic region	30.6
Olfactory nuclei	10.9
Olfactory tubercle	12.2
Periaqueductal gray	8.0
Pons	44.6
Raphe	2.2
Septum	14.5
Substantia innominata	4.7
Substantia nigra	6.6
Superior colliculus	28.3
Thalamus—dorsolateral	43.2
Thalamus—midline dorsal	17.1
Thalamus—ventromedial	3.7
Ventral pallidum	4.9
Ventral tegmental area	2.5
Zona incerta	4.8
Medulla	61.8
Cerebellum	192.7

region was normalized by the global brain mean ^{18}F-FDG uptake for each rat to correct for variability in injected activity. Additional analyses also investigated effects of normalization of brain region uptake by the visual cortex and cerebellum (Fig. 1a). The visual cortex was chosen because it is not affected by disorders that are often studied using BN analysis, such as chronic pain, epilepsy, and depression. The cerebellum is frequently used to normalize FDG uptake in dementia patients because it is minimally affected by disease,[21] serving as a reasonable control region of the brain.

Network Construction

Weighted, undirected inter-subject BNs were constructed; nodes of the network represent brain regions and edges describe the functional relationship between brain regions (Fig. 1b). Mean ^{18}F-FDG uptake values for each brain region from each rat were compiled into separate vectors and the inter-regional Spearman's correlation coefficients were calculated for each pair of brain regions (Fig. 1c). Spearman's correlation is a nonparametric measure of rank correlation that can be applied to relate data with both linear and non-linear associations. Adjacency matrices were constructed with brain regions labeled on the x- and y-axis of the matrix; correlation coefficients, from -1 to 1, comprised the rows and columns of the matrix. This approach resulted in a $[50 \times 50]$ correlation matrix, composed of 2500 association edge weights. BNs that were normalized by the visual cortex or cerebellum resulted in $[49 \times 49]$ correlation matrices, with 2401 association edge weights. All edges were retained for network analysis, since arbitrary thresholding is often associated with a loss of information.[35] All network constructions and analyses were performed in Matlab R2016a (Mathworks; Natick, MA).

Network Stability and Diagnostics

Network diagnostics were calculated using the Brain Connectivity Toolbox (BCT) in Matlab.[34] Node (n) strength, which conveys information about a node's connectivity with the network and the strength of such connections, was calculated by summing the edge weights, w_{ij}, connecting nodes, i and j, of the network.[35] Node strength is commonly defined as the weighted degree, k^W, of a node, i, according to this equation:

$$k_i^W = \sum_{j \in n} w_{ij}. \quad (1)$$

The weighted clustering coefficient describes the neighborhood surrounding each node as defined by the presence of triangle motifs, a common meso-scale structure of complex networks. The weighted clustering coefficient is calculated by finding the average weight, w, of all geometric triangles, t^W, associated with each node, i.[35] Triangles are formed through edges connecting nodes i, j, and h:

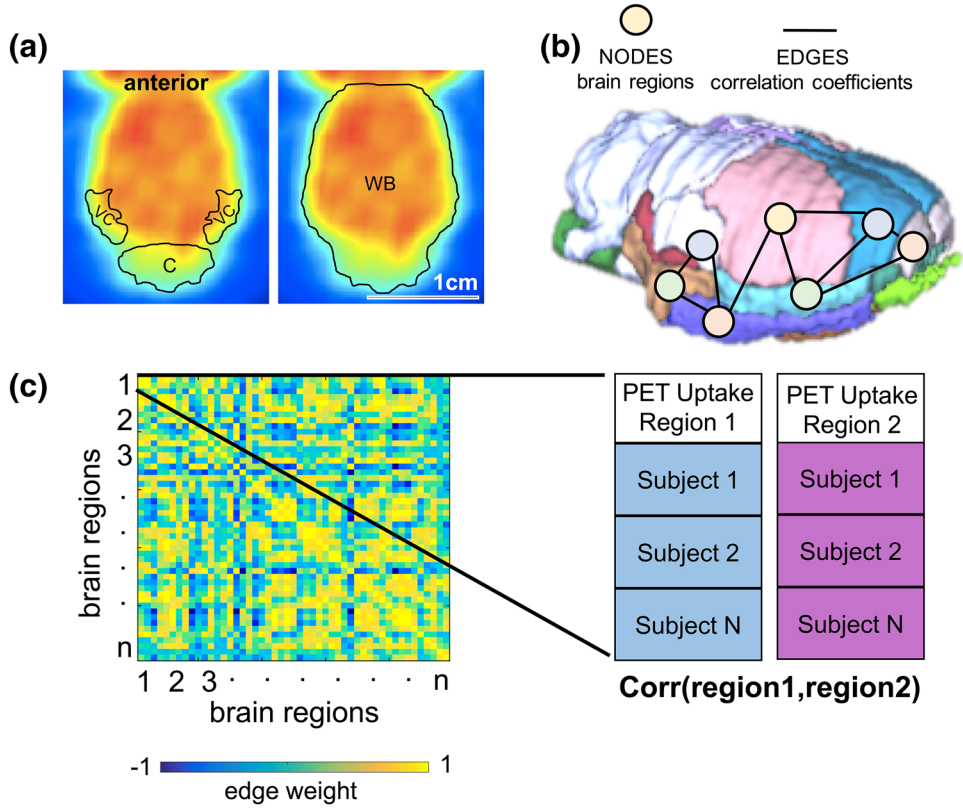

FIGURE 1. Brain networks were constructed by (a) normalizing FDG PET images to uptake in the visual cortex (VC), cerebellum (C), or whole brain (WB), separately, and (b) segmenting FDG PET images into brain regions using the Schwartz rat brain atlas. Brain regions defined the nodes of the network and (c) the inter-subject correlation coefficient between brain regions determined the edge weight.

$$t_i^W = \frac{1}{2}\sum_{j,h\in N}(w_{ij}w_{ih}w_{jh})^{1/3}. \quad (2)$$

The mean triangle weights are normalized by the degree of node i, k_i, to calculate the weighted clustering coefficient, C^W:

$$C^W = \frac{1}{n}\sum_{i\in N}\frac{2t_i^W}{k_i(k_i-1)}. \quad (3)$$

The node strength and local clustering coefficient were analyzed separately for positive and negative edge weights.

Because inter-subject network construction produces a single network per group, additional techniques were employed to measure if, and how, individual subject variation and group size affect the network diagnostics. Node strength and clustering coefficient distributions were investigated for two separate network constructions: (1) networks constructed by varying the numbers of rats to measure how group size affects network properties and (2) networks in which different rats were excluded to analyze the effect of subject-to-subject differences on network diagnostics.

Although inter-subject networks can be constructed from a range of group sizes,[13,20] there is no consensus on the cohort size needed for network stability. So, network stability was assessed across the three BNs with the different normalization approaches (global mean, visual cortex, cerebellum). The clustering coefficient and node strength distributions were calculated for networks constructed using as few as 4, and as many as 18, rats in all possible permutations of order. For example, in one permutation, the smallest group ($n = 4$) included Rats #1–4 and in a second permutation, it was composed of Rats #2–5. Changes in group composition were applied for all group sizes. The critical cohort size was defined as the smallest group size having no significant change in the mean network diagnostic with increased size.

In addition to establishing a critical cohort size, rat-exclusion networks were constructed to assess variability in connectivity that may be introduced by individual rats. Unlike networks constructed for individual subjects from time-varying datasets,[18] inter-

subject networks do not permit analyses of individual variability.[13,20] Therefore, subject-to-subject variability was determined by systematically excluding each rat from the network construction (rat-exclusion networks) and calculating the mean cumulative distribution function for each network diagnostic.[27] Rat-exclusion networks were constructed separately for each normalization technique. The mean and standard deviation of node strength and the clustering coefficient were calculated for all networks.

Modularity and Community Structure

Modularity (Q) measures the degree to which a network is optimally partitioned into non-overlapping modules (m).[31] Nodes that are grouped within the same module are more densely connected to each other and have weaker associations to nodes in other modules. For a weighted network, the modularity is calculated using the number of weighted connections in the graph, l^W, the within-module connection weights, w_{ij}, the chance-expected within module connection weights, e_{ij}, and the resolution parameter, γ; m_i is the module containing node i, and the Kronecker delta function, $\delta_{\mathrm{mi,mj}}$, is 1 if $\mathrm{m_i} = \mathrm{m_j}$ (nodes i and j are in the same module) and 0 otherwise[34]:

$$Q^W = \frac{1}{l^w} \sum_{i,j \in N} [w_{ij} - \gamma e_{ij}] \delta_{m_i m_j} \tag{4}$$

in which the expected connection weights are defined by:

$$e_{ij} = \frac{k_i^w k_j^w}{l^w}. \tag{5}$$

The variable e_{ij} is scaled by the resolution parameter, γ,[32] which can be tuned to identify the coarsest-to-finest partitions of a network.[4]

An asymmetrical modularity measurement is implemented for weighted networks to account for the unequal importance of positive and negative weights in modularity-partition determination.[35] Positive connections contribute to the integration of brain regions into modules, whereas negative connections influence the dissociation of brain regions from modules. Q^W is calculated separately for the positive and negative connections in the weighted network, yielding Q^{W+} and Q^{W-}, which are summed (Q^{W*}). Q^{W-} is reweighted by the total number of network connections[35]:

$$Q^{W*} = Q^+ + \frac{l^{w-}}{l^{w+} + l^{w-}} Q^-. \tag{6}$$

Reweighting Q^- increases the influence of positive weights when calculating Q^{W*} and therefore high-Q network partitions should theoretically have most positive weights within modules and most negative weights between modules.

Due to the non-deterministic nature of community detection calculations, the networks were partitioned over 100 permutations of the community Louvain algorithm in the BCT.[6,35] To evaluate how modularity and network architecture are affected by length-scale, network partitioning was performed at resolution levels from $\gamma = 0$ to $\gamma = 2.0$ in steps of 0.1.[4,6] The community Louvain algorithm outputs both the modularity of the network and the community assignments of each node. Peak modularity was used to determine the unique-consensus clustering; in this analysis, the community structure with peak modularity also corresponded to the most prevalent structure over 100 permutations. The mean network modularity over 100 permutations was compared to the mean modularity of 100 random graph null models with network weight, degree, and strength distributions matched to inter-subject BNs.[35] Community structure was also compared between BNs and random graph null models by calculating the normalized mutual information, a metric that quantifies the similarity between community partitions.[28]

Data and Statistical Analyses

All statistical analyses were performed in R (version 3.2.3, The R Foundation for Statistical Computing), with significance at $p < 0.05$. Edge weight distributions for each network were tested for normality using the Shapiro–Wilk normality test. Network diagnostics were statistically compared across group sizes and ordering permutations using separate one-way ANOVAs for each normalization technique. Differences between networks constructed from increasingly larger group sizes were subjected to Tukey's HSD *post hoc* test. Network diagnostics were compared between whole brain-, visual cortex-, and cerebellum-normalized networks using separate one-way ANOVAs to detect changes in network properties due to normalization technique. Brain and random network modularity were statistically compared across all resolutions tested using a t test to test if the BN properties are different than those of a random network that preserves size and density aspects of the BN.

RESULTS

Network Diagnostics and Group Size

The edge weight distribution for the whole brain-normalized FDG PET BNs reveals an even distribution of positive (1392) and negative (1108) edge weights

throughout the resting state network (Fig. 2). The visual cortex-normalized network has a substantially larger number of positive edges (1843) than negative edges (558) compared to the whole brain-normalized network. The cerebellum-normalized network is primarily composed of positive edges (2309) and has few negative edges (92). All three networks have normal distributions of edge weights ($p < 0.0001$).

Group size influences both node strength and clustering coefficient cumulative distributions for FDG PET resting state networks (Fig. 3). Networks constructed from a very small number of rats (small-*n*), have a higher proportion of positive connections and greater mean clustering coefficients and node strengths compared to networks using a higher number of rats (large-*n*). Analysis over all 105 possible permutations of rat ordering reveals that the mean node strength and clustering coefficients stabilize for networks constructed from 10 or more rats across the normalization techniques and diagnostics tested. Clustering coefficient and node strength are most altered by group size in the whole brain-normalized network, and to a lesser degree in the other networks (Fig. 3). Therefore, the results pertaining to group size specifically focus on the whole brain-normalized network.

The mean clustering coefficient for positive connections decreases between whole brain-normalized networks with 9–10 rats ($p = 0.028$). However, the clustering coefficient is not different between groups using 10 or 11 rats ($p = 0.272$) (Fig. 3). For negative connections, clustering coefficient is less affected by group size and stabilizes at groups between 5 and 6 rats ($p = 0.824$). The mean node strength for positive connections stabilizes between 10 and 11 rats ($p = 0.082$) and between groups using 9 and 10 rats ($p = 0.081$) for negative connections. There are no differences between network diagnostics for group sizes of 10 and 11 rats in the visual cortex- and cerebellum-normalized networks ($p > 0.05$), suggesting that all networks are stable at this group size and larger.

At this stable group size, the node strength and clustering coefficient amongst positive connections are greater in the cerebellum- and visual cortex-normalized networks compared to the whole brain-normalized ($p < 0.00001$). Amongst negative connections, the clustering coefficient is lower in the cerebellum-normalized network compared to the whole brain and visual cortex-normalized networks ($p < 0.00001$). The clustering coefficient for the whole brain- and visual cortex-normalized networks are not significantly different ($p = 0.999$). The node strength amongst negative connections is greater in the whole brain-normalized network compared to both the visual cortex-normalized and cerebellum-normalized networks ($p < 0.00001$).

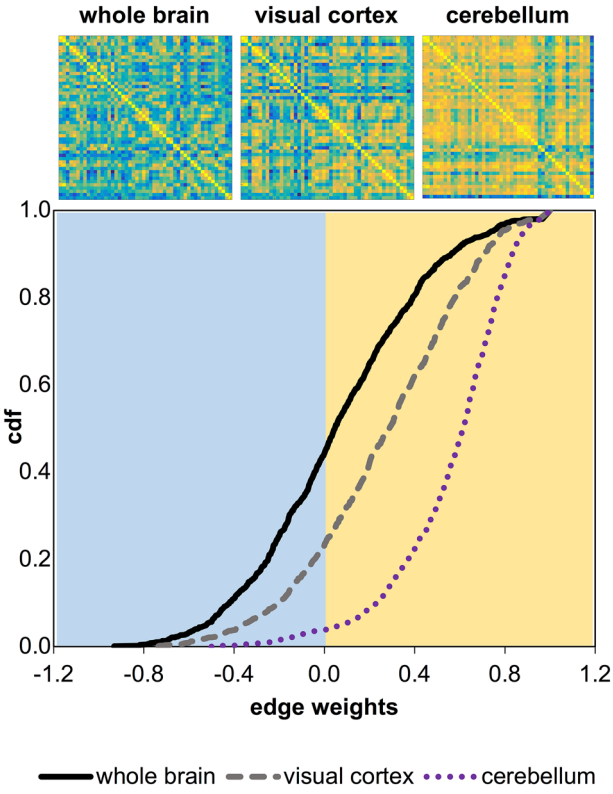

FIGURE 2. The whole brain-, visual cortex-, and cerebellum-normalized networks are shown with the cumulative distribution function (cdf) of edge weights for each network.

Community Structure of PET Networks

FDG PET networks exhibit multi-scale community structure, as evidenced by network partitioning across the range of resolutions tested ($\gamma = 0$–2.0) (Fig. 4). Across normalization strategies, modularity decreases as γ is increased, suggesting weaker partitioning of the network at higher resolutions compared to lower resolutions. FDG PET network modularity is greater than randomized networks when compared across all values of $\gamma > 0.1$ in the whole brain- ($p < 0.00001$), visual cortex- ($p < 0.00001$), and cerebellum-normalized ($p = 0.0001$) networks (Fig. 4a). However, the modularity of cerebellum-normalized networks is not different from random networks for $\gamma < 0.8$.

Over 100 permutations, all partitions of the whole brain-normalized and visual cortex-normalized networks exhibit a 2-module structure at low resolutions, like $\gamma = 0.5$ (Fig. 4c). However, all nodes in the cerebellum-normalized network are assigned to a single module. At higher resolutions, such as $\gamma = 2$, a greater number of communities form in all three networks (Fig. 4c). The difference in modularity peaks for all three normalized-networks in the range of $\gamma = 0.7$–1.0, demonstrating that FDG PET networks in this range

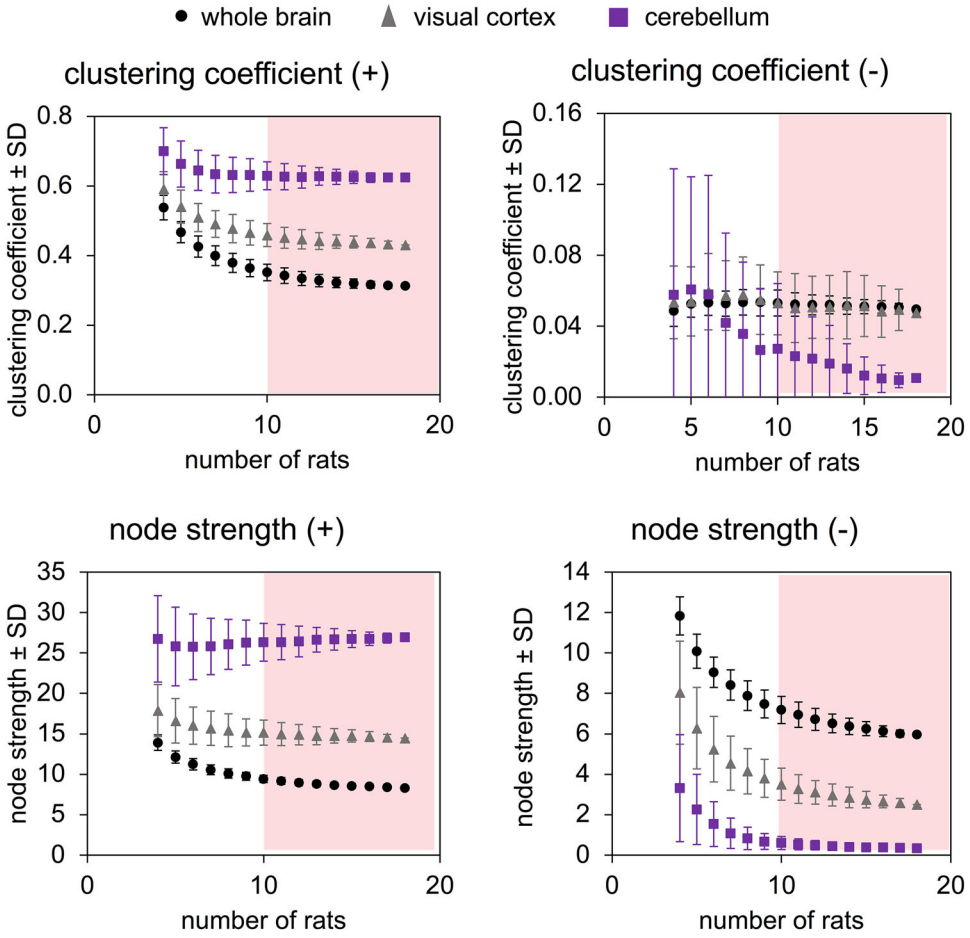

FIGURE 3. The average clustering coefficient and node strength calculated for networks that include groups sized of 4 rats to 18 rats, shown separately for positive (+) and negative (–) edges. Diagnostics of FDG PET networks are stable when 10 or more rats are used in network construction (denoted by pink shading).

are most distinct from their randomized counterparts (Fig. 4a). Normalized mutual information is also minimized in this range (Fig. 4b), confirming the lack of similarity in community structure between brain and randomized networks.

Interestingly, the three differently normalized networks have almost identical community structures at $\gamma = 1.0$ (Fig. 4c), indicating that there may be a consensus in FDG PET network structure at this resolution. Anatomical analysis reveals that 46 of the 50 brain regions in the network are assigned to the same communities across all three normalization techniques (Fig. 4d). Four regions, including the medulla, somatosensory cortex, cingulate cortex, and frontal association cortex are differently assigned between at least two of the three networks. Module I is composed of anterior cortical regions, caudate/putamen (CP), nucleus accumbens (N), and pallidal nuclei. Module II contains cortical regions, including the visual, auditory, and motor cortices, the hypothalamus (Hy), and amygdala (A). The somatosensory (S), cingulate (C), and frontal association cortices have shared affiliations between modules I and II. The largest module (III) includes the hippocampus (H) and thalamic (T) regions, upper brainstem regions, mesencephalon, and cerebellum. The medulla affiliates with both modules II and III.

Hierarchical Network Organization

The whole brain-normalized network is the most modular and has the strongest hierarchical community structure (Fig. 4). At a low network resolution ($\gamma = 0.5$), the network is composed of two communities, primarily defined by the anterior or posterior anatomical location of a brain region (Fig. 5). Tuning the resolution to $\gamma = 0.7$ uncovers a third, small community that is located between the anterior and posterior modules. The new module includes the amygdala and temporal association, visual, auditory, and entorhinal cortices. Further tuning to $\gamma = 1.0$ expands that module to include the hypothalamus, motor cor-

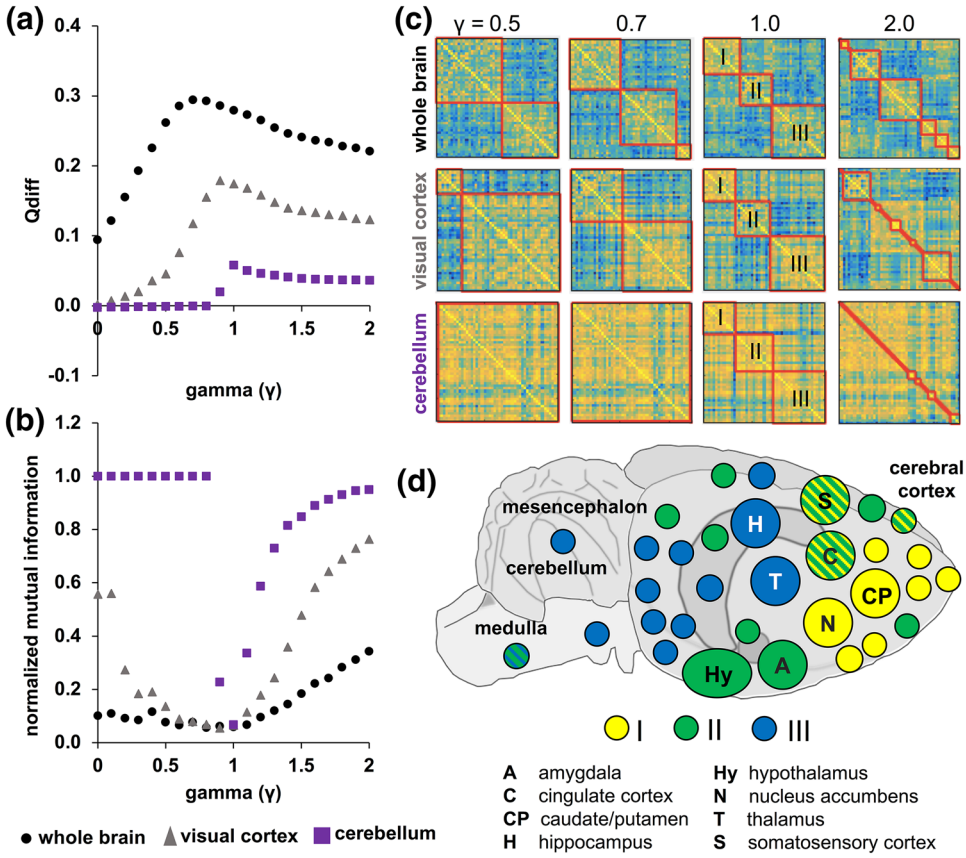

FIGURE 4. Normalization technique (a) affects the value of Q_{diff} across multiple resolutions. The difference between the whole brain-normalized and randomized networks, Q_{diff}, is larger than both visual cortex- and cerebellum-normalized networks across all resolutions tested ($p<0.00001$). The peak Q_{diff} is similar for the three networks (γ=0.7–1.0). (b) Normalized mutual information between brain networks and randomized networks is minimized within the same range. (c) The networks have multi-scale community structure and are composed of three modules at γ=1. (d) At γ=1.0, there are strong associations between the caudate/putamen, nucleus accumbens, and prefrontal regions (I), hypothalamus, amygdala, and posterior cortex (II), and thalamus, hippocampus, pons, and mesencephalon (III). The medulla, somatosensory cortex, cingulate cortex, and frontal association cortex are differently assigned in the three networks and are shaded to designate affiliation with two modules. Labeled and enlarged nodes are included for orientation.

tex, and insular cortex. These regions primarily disassociate from the anterior module and the posterior module remains consistent across $\gamma = 0.5$–1.0.

Increasing the resolution to $\gamma = 2.0$ reveals six smaller modules (Fig. 5). The posterior and amygdala modules are largely consistent from $\gamma = 1.0$ to $\gamma = 2.0$ and the smaller modules are derived from the less stable anterior module (Fig. 5). The four small modules include the caudate/putamen and globus pallidus, nucleus accumbens core and anterior cortex, nucleus accumbens shell and somatosensory cortex, and lateral hypothalamus, substantia nigra, and ventral tegmental area. Decomposition into smaller modules splits the shell and core components of the nucleus accumbens and medial/lateral hypothalamus into separate modules (Fig. 5). Also, the cingulate cortex and the ventromedial portion of the thalamus are assigned to their own modules.

DISCUSSION

This study used community detection and network diagnostic measurements to define properties of inter-subject FDG PET networks. Although PET inter-subject networks have been used to describe altered brain function in Alzheimer's disease, epilepsy, and during astrocyte stimulation with ceftriaxone,[30,42,44] the basic characteristics and structure of such networks have not been studied. This study found that the stability of network properties depends on the size of the group by detecting that node strength and clustering coefficient are altered by cohort size (Fig. 3). Further, the minimum group size for which FDG PET inter-subject network analyses are stable across different normalization techniques was determined here ($n = 10$) to be similar to the group size of previous inter-subject network studies that included 9–10 rodents in each group.[13,44] However, while those larger group sizes are

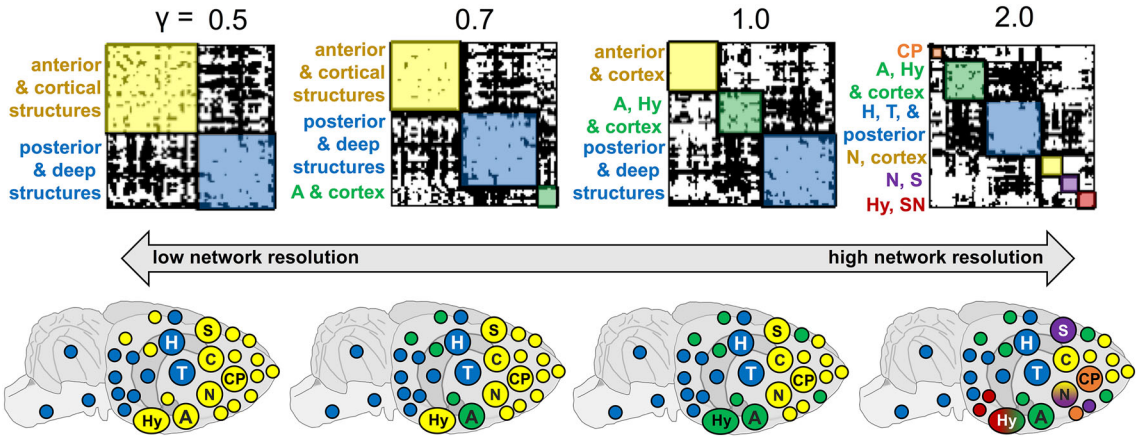

FIGURE 5. In the whole brain-normalized network, there is multi-scale community structure that exhibits a hierarchical pattern. At a low network resolution (γ=0.5), the brain is partitioned into 2 modules: the anterior/cortical structures and posterior/deep structures. When the brain network is most different from a random network (peak Q_{diff}, γ=0.7–1.0), the network has 3 modules: consistent anterior and posterior communities, and a third community that includes the hypothalamus, amygdala, and posterior cortical regions. At a high network resolution (γ=2.0) the brain is partitioned into 6 modules, which separates the sub-regions of two larger structures (designated by partially shaded circles, which represent 2 nodes), including the shell and core of the nucleus accumbens and the medial and lateral hypothalamus, which associates with the substantia nigra (SN).

statistically powered to detect differences in brain activity between control and ketamine or ceftriaxone treatment groups,[13,44] they did not perform network-specific analyses of group size. Although node strength and clustering coefficient metrics are modified by differently normalized networks (Fig. 3), some of these disparities may be connectivity density-dependent and not represent true topological differences (Fig. 2).[16,40] Techniques such as the minimum spanning tree can be used to test for density and connectivity-dependent differences between networks because they are not sensitive to connection strength (Supplemental Figure 1).[40]

These stable FDG PET inter-subject networks also have organized, modular structure, which is a key feature of BNs.[29] Modularity is up to 20 times greater in FDG PET networks than in corresponding randomized networks (Fig. 4a), suggesting there is strong community structure in the network that is not expected to occur by random chance.[29] The enduring community structure that is observed across length scales (Fig. 4a) implies that brain metabolism is organized to achieve segregated information processing,[38] which aligns with blood oxygenation[2,12] and electrical measurements[22] of brain activity. The difference between brain and randomized network modularity peaks in the range of $\gamma = 0.7$–1.0 (Fig. 4b), with greatest modularity in the whole brain-normalized network and lower modularity in the visual cortex- and cerebellum-normalized networks. The modularity of the whole brain-normalized and visual cortex-normalized networks agrees with previous findings for fully-connected, weighted BNs [5] and peak modularity for rat BNs.[3]

Despite differences in network diagnostics and modularity, the different normalization techniques produce almost identical community structures in the range of peak Q_{diff}, particularly at $\gamma = 1.0$ (Fig. 4c). Consistent community structure and node assignments within the structure demonstrate that normalization strategy does *not* substantially impact network structure within peak Q_{diff} ranges. The consensus network model (Fig. 4d) contains strong connectivity between anterior cortical and subcortical regions (module I), subcortical/posterior regions (module III), and midbrain subcortical and cortical regions (module II) (Fig. 4d). fMRI BNs in the rat identify particularly strong connectivity between the prefrontal/cingulate cortices, caudate/putamen, nucleus accumbens, septum, and amygdala,[37] similar to module I of the consensus model. However, the three normalized networks studied here suggest that the amygdala does not strongly associate with these coupled brain regions in metabolic networks (Fig. 4c).

Although community structure is consistent at $\gamma = 1.0$, network structure is not consistent outside of peak Q_{diff}; it is recommended that the normalization strategy be selected based on the biological questions under study and with consideration of any anesthetics or sedatives used.[21,24] For example, microPET FDG images acquired in a rodent seizure model are normalized to the pons because the initiating agent does not affect the metabolic rate of that brain region.[24] Since normalization by global brain uptake is the most

widely used scaling technique for FDG PET images,[15,23,42] it was a focus of the current analysis.

Evaluating community structure in the whole brain-normalized network revealed strong hierarchical composition, with consensus in structure between different network scales. At $\gamma = 0.5$, the network is partitioned into two modules, which are primarily defined by anterior or posterior location in the brain (Fig. 5). This finding is consistent with studies of both structural and functional BNs, which identify strong connectivity between spatially-proximate brain regions,[38] particularly for communities with many nodes (low resolutions of gamma).[25] This may be a function of non-trivial constraints on the embedding of BNs within a rodent or human skull.[10] Brain anatomy has been hypothesized as optimized for minimum connection distance between functionally coordinated regions while also maintaining some long-distance connections that act as "short-cuts" between distant areas of the brain.[38]

In this work, the connectivity within the posterior module is maintained when sweeping from $\gamma = 0$ to $\gamma = 2.0$, dividing into a medium and a small module at high network resolutions (Fig. 5). The anterior module is much less stable than the posterior module, splitting into two communities at $\gamma = 0.7$ and giving rise to many smaller communities at higher resolutions. Resting state fMRI has also identified multiple cortical communities at higher network resolutions in both humans and rats.[12,29] However, PET and fMRI BNs are inherently constrained by their resolution limits and it remains challenging to study small modules. Therefore, imaging studies can be complemented by other approaches, such as an aggregated network of > 16,000 histological tract tracing studies.[7] The tract network suggests that the rat cortex strongly subdivides into four modules when examined at the resolution of neurons and axons.

This study supports the presence of multi-scale modularity in inter-subject FDG PET networks and consistency in community structure across different normalization techniques. FDG PET BNs have a hierarchical community structure, with a consistent module composed of posterior and deep brain structures and a less stable module with anterior and cortical brain regions. In addition, a technique to identify the appropriate group size for stable FDG PET networks is described; in this study, group sizes of at least 10 rodent subjects are needed to minimize data variability that may be present in small, unstable networks. Further studies are needed to investigate size-stability in the context of a disease and/or drug perturbation, as well as effects of these changes on multi-scale modularity. Studies that use FDG PET networks to compare disease states may also benefit from statistical thresholding to identify the strongest sub-circuits within the network and filter out noisy or spurious connections.[16] However, filtered networks may suffer from complete disconnections between a node and the larger network (Supplemental Figure 2) and/or isolation of nodes with only positive or negative connections. Such network detachments are not present in the fully-connected correlation matrices analyzed in the present study. Although additional studies are needed to fully characterize these resting-state networks, this is the first study to demonstrate multi-scale community structure in FDG PET BNs.

ELECTRONIC SUPPLEMENTARY MATERIAL

The online version of this article (https://doi.org/10.1007/s10439-018-2022-x) contains supplementary material, which is available to authorized users.

ACKNOWLEDGMENTS

The authors thank Eric Blankemeyer for his assistance with PET imaging, Dr. Danielle Bassett for helpful conversations regarding modularity, and Dr. Blythe Phillips for consultation when developing the dexmedetomidine sedation protocol. This project was supported by funding from the Catherine D. Sharpe Foundation, the Oral and Maxillofacial Surgery Foundation, the Oral and Maxillofacial Surgery Schoenleber Research Fund from the University of Pennsylvania School of Dental Medicine, and a training grant from NIH/NIAMS (T32-AR007132).

CONFLICT OF INTEREST

The authors have no conflicts of interest to disclose.

REFERENCES

[1]Avants, B. B., N. J. Tustison, G. Song, P. A. Cook, A. Klein, and J. C. Gee. A reproducible evaluation of ANTs similarity metric performance in brain image registration. *Neuroimage* 54:2033–2044, 2011.

[2]Baliki, M. N., P. C. Chang, A. T. Baria, M. V. Centeno, and A. V. Apkarian. Resting-state functional reorganization of the rat limbic system following neuropathic injury. *Sci. Rep.* 4:6186, 2014.

[3]Bettinardi, R. G., N. Tort-Colet, M. Ruiz-Mejias, M. V. Sanchez-Vives, and G. Deco. Gradual emergence of spontaneous correlated brain activity during fading of general anesthesia in rats: evidences from fMRI and local field potentials. *Neuroimage* 114:185–198, 2015.

[4]Betzel, R. F., and D. S. Bassett. Multi-scale brain networks. *Neuroimage* 7:446–451, 2016.

[5]Betzel, R. F., M. Fukushima, Y. He, X. N. Zuo, and O. Sporns. Dynamic fluctuations coincide with periods of high and low modularity in resting-state functional brain networks. *Neuroimage* 127:287–297, 2016.
[6]Blondel, V. D., J.-L. Guillaume, R. Lambiotte, and E. Lefebvre. Fast unfolding of communities in large networks. *J. Stat. Mech. Theory Exp.* 2008. https://doi.org/10.1088/1742-5468/2008/10/p10008.
[7]Bota, M., O. Sporns, and L. W. Swanson. Architecture of the cerebral cortical association connectome underlying cognition. *Proc. Natl. Acad. Sci. USA* 112:E2093–E2101, 2015. https://doi.org/10.1073/pnas.1504394112.
[8]Braun, U., A. Schäfer, H. Walter, S. Erk, N. Romanczuk-Seiferth, L. Haddad, J. I. Schweiger, O. Grimm, A. Heinz, H. Tost, A. Meyer-Lindenberg, and D. S. Bassett. Dynamic reconfiguration of frontal brain networks during executive cognition in humans. *Proc. Natl. Acad. Sci. USA* 112:11678–11683, 2015.
[9]Bullmore, E. T., and O. Sporns. Complex brain networks: graph theoretical analysis of structural and functional systems. *Nat. Rev. Neurosci.* 10:186–198, 2009.
[10]Bullmore, E., and O. Sporns. The economy of brain network organization. *Nat. Rev. Neurosci.* 13:336–349, 2012.
[11]Chen, Z. J., Y. He, P. Rosa-Neto, J. Germann, and A. C. Evans. Revealing modular architecture of human brain structural networks by using cortical thickness from MRI. *Cereb. Cortex* 18:2374–2381, 2008.
[12]D'Souza, D. V., E. Jonckers, A. Bruns, B. Kunnecke, M. Von Kienlin, A. Van Der Linden, T. Mueggler, and M. Verhoye. Preserved modular network organization in the sedated rat brain. *PLoS ONE* 9:e106156, 2014.
[13]Dawson, N., M. McDonald, D. J. Higham, B. J. Morris, and J. A. Pratt. Subanesthetic ketamine treatment promotes abnormal interactions between neural subsystems and alters the properties of functional brain networks. *Neuropsychopharmacology* 39:1786–1798, 2014.
[14]De Haan, W., W. M. Van der Flier, T. Koene, L. L. Smits, P. Scheltens, and C. J. Stam. Disrupted modular brain dynamics reflect cognitive dysfunction in Alzheimer's disease. *Neuroimage* 59:3085–3093, 2012.
[15]Di, X., B. B. Biswal, and A. D. N. Initiative. Metabolic brain covariant networks as revealed by FDG-PET with reference to resting-state fMRI networks. *Brain Connect.* 2:275–283, 2012.
[16]Dimitriadis, S. I., C. Salis, I. Tarnanas, and D. E. Linden. Topological filtering of dynamic functional brain networks unfolds informative chronnectomics: a novel data-driven thresholding scheme based on orthogonal minimal spanning trees (OMSTs). *Front. Neuroinform.* 11:28, 2017.
[17]Garcia, D. V., C. Casteels, A. J. Schwarz, R. A. J. O. Dierckx, M. Koole, and J. Doorduin. A standardized method for the construction of tracer specific PET and SPECT rat brain templates: validation and implementation of a toolbox. *PLoS ONE* 10:e0143900, 2015. https://doi.org/10.1371/journal.pone.0122363.
[18]Gonçalves, S. I., J. C. De Munck, P. J. W. Pouwels, R. Schoonhoven, J. P. A. Kuijer, N. M. Maurits, J. M. Hoogduin, E. J. W. Van Someren, R. M. Heethaar, and F. H. Lopes Da Silva. Correlating the alpha rhythm to BOLD using simultaneous EEG/fMRI: inter-subject variability. *Neuroimage* 30:203–213, 2006.
[19]Hagmann, P., L. Cammoun, X. Gigandet, R. Meuli, C. J. Honey, J. Van Wedeen, and O. Sporns. Mapping the structural core of human cerebral cortex. *PLoS Biol.* 6:1479–1493, 2008.
[20]He, Y., Z. J. Chen, and A. C. Evans. Small-world anatomical networks in the human brain revealed by cortical thickness from MRI. *Cereb. Cortex* 17:2407–2419, 2007.
[21]Jeong, Y., S. S. Cho, J. M. Park, S. J. Kang, and J. S. Lee. PET findings in frontotemporal dementia: an SPM analysis of 29 patients. *J. Nucl. Med.* 46:233–239, 2005.
[22]Khambhati, A. N., K. A. Davis, B. S. Oommen, S. H. Chen, T. H. Lucas, B. Litt, and D. S. Bassett. Dynamic network drivers of seizure generation, propagation and termination in human neocortical epilepsy. *PLoS Comput. Biol.* 11:1–19, 2015.
[23]Kim, C.-E., Y. K. Kim, G. Chung, J. M. Jeong, D. S. Lee, J. Kim, and S. J. Kim. Large-scale plastic changes of the brain network in an animal model of neuropathic pain. *Neuroimage* 98:203–215, 2014.
[24]Kornblum, H. I., D. M. Araujo, A. J. Annala, K. J. Tatsukawa, M. E. Phelps, and S. R. Cherry. In vivo imaging of neuronal activation and plasticity in the rat brain by high resolution positron emission tomography (microPET). *Nat. Biotechnol.* 18:655–660, 2000.
[25]Lohse, C., D. S. Bassett, K. O. Lim, and J. M. Carlson. Resolving anatomical and functional structure in human brain organization: identifying mesoscale organization in weighted network representations. *PLoS Comput. Biol.* 10: e1003712, 2014.
[26]Lundgaard, I., B. Li, L. Xie, H. Kang, S. Sanggaard, J. D. R. Haswell, W. Sun, S. Goldman, S. Blekot, M. Nielsen, T. Takano, R. Deane, and M. Nedergaard. Direct neuronal glucose uptake heralds activity-dependent increases in cerebral metabolism. *Nat. Commun.* 6:6807, 2015.
[27]Mechelli, A., W. D. Penny, C. J. Price, D. R. Gitelman, and K. J. Friston. Effective connectivity and intersubject variability: using a multisubject network to test differences and commonalities. *Neuroimage* 17:1459–1469, 2002.
[28]Meilă, M. Comparing clusterings-an information based distance. *J. Multivar. Anal.* 98:873–895, 2007.
[29]Meunier, D., R. Lambiotte, and E. T. Bullmore. Modular and hierarchically modular organization of brain networks. *Front. Neurosci.* 4:1–11, 2010.
[30]Morbelli, S., A. Drzezga, R. Perneczky, G. B. Frisoni, A. Caroli, B. N. M. van Berckel, R. Ossenkoppele, E. Guedj, M. Didic, A. Brugnolo, G. Sambuceti, M. Pagani, E. Salmon, and F. Nobili. Resting metabolic connectivity in prodromal Alzheimer's disease. A European Alzheimer Disease Consortium (EADC) project. *Neurobiol. Aging* 33:2533–2550, 2012.
[31]Newman, M. E. J. Analysis of weighted networks. *Phys. Rev. E* 70:1–9, 2004.
[32]Reichardt, J., and S. Bornholdt. Statistical mechanics of community detection. *Phys. Rev. E* 74:1–14, 2006.
[33]Riedl, V., K. Bienkowska, C. Strobel, M. Tahmasian, T. Grimmer, S. Forster, K. J. Friston, C. Sorg, and A. Drzezga. Local activity determines functional connectivity in the resting human brain: a simultaneous FDG-PET/fMRI study. *J. Neurosci.* 34:6260–6266, 2014.
[34]Rubinov, M., and O. Sporns. Complex network measures of brain connectivity: uses and interpretations. *Neuroimage* 52:1059–1069, 2010.
[35]Rubinov, M., and O. Sporns. Weight-conserving characterization of complex functional brain networks. *Neuroimage* 56:2068–2079, 2011.
[36]Schwarz, A. J., A. Danckaert, T. Reese, A. Gozzi, G. Paxinos, C. Watson, E. V. Merlo-Pich, and A. Bifone. A stereotaxic MRI template set for the rat brain with tissue

class distribution maps and co-registered anatomical atlas: application to pharmacological MRI. *Neuroimage* 32:538–550, 2006.
[37]Schwarz, A. J., A. Gozzi, and A. Bifone. Community structure in networks of functional connectivity: resolving functional organization in the rat brain with pharmacological MRI. *Neuroimage* 47:302–311, 2009.
[38]Sporns, O., D. R. Chialvo, M. Kaiser, and C. C. Hilgetag. Organization, development and function of complex brain networks. *Trends Cogn. Sci.* 8:418–425, 2004.
[39]Stoessl, A. J. Glucose utilization: still in the synapse. *Nat. Neurosci.* 20:382–384, 2017.
[40]Tewarie, P., E. van Dellen, A. Hillebrand, and C. J. Stam. The minimum spanning tree: an unbiased method for brain network analysis. *Neuroimage* 104:177–188, 2015.
[41]van den Heuvel, M. P., H. E. Hulshoff, and H. E. H. Pol. Exploring the brain network: a review on resting-state fMRI functional connectivity. *Eur. Neuropsychopharmacol.* 20:519–534, 2010.
[42]Vanicek, T., A. Hahn, T. Traub-Weidinger, E. Hilger, M. Spies, W. Wadsak, R. Lanzenberger, E. Pataraia, and S. Asenbaum-Nan. Insights into intrinsic brain networks based on graph theory and PET in right- compared to left-sided temporal lobe epilepsy. *Sci. Rep.* 6:28513, 2016.
[43]Yushkevich, P. A., J. Piven, H. C. Hazlett, R. G. Smith, S. Ho, J. C. Gee, and G. Gerig. User-guided 3D active contour segmentation of anatomical structures: significantly improved efficiency and reliability. *Neuroimage* 31:1116–1128, 2006.
[44]Zimmer, E. R., M. J. Parent, D. G. Souza, A. Leuzy, C. Lecrux, H.-I. Kim, S. Gauthier, L. Pellerin, E. Hamel, and P. Rosa-Neto. [18F]FDG PET signal is driven by astroglial glutamate transport. *Nat. Neurosci.* 20:393–395, 2017.